Macromolecules
ARTICLE

Macromolecules **2010**, *43*, 9837–9847 **9837**
DOI: 10.1021/ma101898c

Conformations of Silica−Poly(ethylene−propylene) Nanocomposites

Klaus Nusser,* Susanne Neueder, Gerald J. Schneider,* Mathias Meyer, Wim Pyckhout-Hintzen, Lutz Willner, Aurel Radulescu, and Dieter Richter

Institut für Festkörperforschung, Neutronenstreuung, and Jülich Centre for Neutron Science, Forschungszentrum Jülich GmbH, 52425 Jülich, Germany

Received August 18, 2010; Revised Manuscript Received October 25, 2010

ABSTRACT: By the use of small angle neutron scattering, the chain conformation in a polymer nanocomposite was studied as a function of the nanoparticle fraction for two different molecular weights. A repulsive system was realized in mixing poly(ethylene−propylene) and hydrophobically modified silica. All nanocomposite SANS data exhibit a pronounced scattering peak at intermediate momentum transfers, which is closely connected with the particle structure. Even under contrast matching conditions, the hydrophobic surface layer of the nanoparticles was found to contribute significantly to the scattering signal. In particular, in the short chain matrix the peak origin is exclusively related to direct particle scattering. In the long chain matrix, an additional peak contribution is present. Possible origins include void correlation scattering or polymer correlation scattering. We show unambiguously that the conformation of short chains with a molecular weight of 3000 g/mol is not visibly disturbed by the presence of the nanoparticles. In contrast to that a polymer matrix with 50 000 g/mol chains is affected by the particle presence. The chain radius of gyration R_g decreases.

Introduction

Reinforcement of polymers by inorganic particles has been known and used for a long time. Nevertheless, a detailed molecular understanding of the microscopic mechanisms is still a challenge. With the availability of nanosized filler particles with a wide variety of surface coatings, both scientific and industrial research on the subject of polymer nanocomposites were greatly enhanced. In particular, attention has been dedicated to the investigation of the polymer structure in the presence of nanoparticles. Unfortunately, results in the literature are still very ambivalent. In simulations, both the chain conformation dependence on energetic filler−polymer interaction as well as on chain size R_{pol} vs particle size R_{part} were studied.[1−7] As long as the energetic filler−polymer interaction was not unrealistically high, the main results were qualitatively governed by the polymer−filler size ratio $\Psi = R_{pol}/R_{part}$. In general, three different regimes were accessed by the different simulations, $\Psi < 1$, $\Psi \approx 1$, and $\Psi > 1$. The main results of representative simulations by Termonia,[1] Sung,[2] Vacatello,[3,4] Sharaf,[5] and Picu and Ozmusul[6,7] in their respective regimes will be briefly summarized in order to illustrate the existing discrepancies.

- For $\Psi < 1$, the results are quite in agreement with each other despite different simulation assumptions and model systems. Termonia, Picu, and Dionne find that the chain size is not affected at all in this regime. Sharaf's result indicates a decrease of the chain size, but only on the order of 2%. Thus, the chain size is hardly affected by the presence of the nanofillers, as long as it is small compared to the filler size.
- The situation is different, when $\Psi \approx 1$. In this regime, Picu finds a decrease of the average radius of gyration R_g for all filler fractions Φ. This is in accordance with the results by Vacatello, who uses Monte Carlo simulations in realistically dense systems and always finds a decrease of R_g independent of the specific chain molecule (PE, PDMS). Sharaf also observes a significant decrease of the chain size at filler fractions $\Phi \geq 0.10$ using polyethylene (PE) chains with 1000 skeletal bonds. (At low filler fractions $\Phi < 0.04$, he reports a swelling of the chain; these filler fractions are not of interest in this context, however.) In contrast to these findings, Termonia's Monte Carlo simulations (using a technique introduced by Pakula et al.), were also performed for a polyethylene system, but predict hardly affected chain sizes at $\Psi \approx 1$ for high filler fractions.
- The biggest discrepancies arise in the $\Psi > 1$ regime. Here, the simulations by Termonia yield a significant swelling of the chain size in the presence of the nanoparticles (by more than 10%); in particular, this is also true at high filler fractions $\Phi \geq 0.20$. This is in agreement with the findings of Sung. The latter work investigates polymers in porous media, where in principle the porous medium is considered as hard spheres that percolate above the percolation threshold (≈0.3 in all considered scenarios). Moreover, Sharaf also reports significant chain swelling for $\Psi < 1$, but only for small Φ. For $\Phi > 0.10$ all computed systems finally exhibit a chain size decrease. An analogous decrease of R_g is also reported by Vacatello for $\Phi \geq 0.10$.

The subject has also been addressed experimentally by scattering experiments. Nakatani measured an R_g-decrease in a system of PDMS and trimethylsilyl-treated fillers, when polymer and particle size were of the same order, and an increase, when the chains were significantly longer.[8] Mackay et al. showed the swelling of PS chains in the presence of nanofillers ($\Psi > 1$),[9] whereas Sen et al. observed unchanged chain conformations in PS-silica nanocomposites[10] over a wide range of PS molecular weigths ($\Psi \approx 1-3$). In the latter work, a pronounced polymer correlation peak at intermediate Q was found. To our knowledge, the regime $\Psi \ll 1$ has not been experimentally addressed in detail for high filler fractions Φ.

*Corresponding authors. E-mail: (K.N.) k.nusser@fz-juelich.de; (G.J.S.) g.j.schneider@fz-juelich.de.

Published on Web 11/16/2010

Since so many different observations exist in literature, we chose to approach the topic with a well-defined model system with negligible energetic particle−polymer and particle−particle interactions. This will enable a separation of confinement effects of merely geometrical and excluded volume nature vs those of energetic nature in more complicated systems.

Furthermore, we demonstrate that vigilance needs to be applied, when polymer quantities are extracted from experimental nanocomposite scattering data. In particular, we will emphasize that even under best-possible matching conditions filler particles may have a significant scattering contribution. Our investigation is therefore concerned with an accurate nanoparticle characterization and particularly the quantification of a direct particle scattering contribution. It will become clear that for hydrophobically modified nanoparticles this procedure is necessary, when composites with high particle volume fractions are studied.

The present study uses small angle neutron scattering (SANS) in order to contribute to a better understanding of the chain conformation in polymer nanocomposites. Composites of high filler fractions of silica particles, covered with a hydrophobic surface layer, in a hydrophobic polymer matrix (poly(ethylene-propylene)) are investigated. This constitutes a model system for a polymer−particle nanocomposite with nonattractive interactions.

The system is studied for two different molecular weights M_w, which were chosen so that $\Psi \ll 1$ and $\Psi \gtrsim 1$. The first choice is primarily meant to structurize the general conclusions from simulations. The higher molecular weight on the other hand was chosen to contribute to a better understanding of the $\Psi \gtrsim 1$ regime, where great discrepancies arise from the different simulative approaches.

For both molecular weights, we find that the chain statistics is not affected and remains Gaussian. The polymer radius of gyration is also unchanged, when the chain size is much smaller than the particle size. When the chain size becomes comparable to the particle size, a decrease of the radius of gyration at high filler fractions is observed. Moreover, in all samples an identical scattering peak at intermediate Q values is found, which is closely connected to the particle structure. All of the scattered peak intensity directly originates from the particle core−shell contrast in the short matrix. In the long matrix, evidence for an additional scattering contribution from voids or polymer correlations is found.

The paper is organized as follows. In the Experimental Section, the material system is introduced, and the SANS method is presented. In the next section, Theoretical Background, a brief overview over the necessary scattering functions for the data modeling is given. Then in the Results and Discussion, the experimental results are presented and discussed. First, a characterization of the unfilled polymer matrices and of the used particles was performed separately. The primary particle structure and average scattering length density is extracted from measurements in dilute solution. Then, the nanocomposite SANS data are presented, where always the average polymer scattering length density is equal to the average particle scattering length density. Before final quantitative conclusions are drawn from these data, however, we present an ancillary measurement in order to quantifiy the scattering contribution from the particle core−shell contrast. This is achieved by measuring a sample with high particle volume fraction in toluene solution, where the average toluene scattering length density is equal to the particles', i.e. under the same contrast conditions that prevail in the nanocomposites. With this knowledge, the direct scattering contribution from the particles is removed from the SANS data. The remaining signal is then compared to the data from the unfilled melts, and differences are discussed in detail.

Table 1. Molecular Characteristics of PEP Polymers

sample	M^a (g/mol)	M_w/M_n
h-PEP3k	2980	1.04
d-PEP3k	3400	1.04
h-PEP50k	48900	1.02
d-PEP50k	49800	1.02

[a] M_n for PEP3k, M_w for PEP50k polymers.

Experimental Section

Materials. The model nanocomposite used in this work consists of poly(ethylene-*alt*-propylene) (=:PEP) as an apolar polymer component and hydrophobically modified silica from Nissan Chemical as filler component. Thus, a nanocomposite with dominantly repulsive interaction is realized.

Two pairs of deuterated and hydrogenated PEP samples with different molecular weights, h-PEP3k, d-PEP3k and h-PEP50k, d-PEP50k were chosen as the soft component. The four PEP polymers were synthesized from parent polyisoprenes, h- and d-PI, by catalytic hydration (deuteration) using a conventional $Pd/BaSO_4$ catalyst. The corresponding polyisoprenes were prepared by anionic polymerization of isoprene (d-isoprene) monomer, with t-butyllithium as initiator and benzene as polymerization solvent. The obtained microstructure consists of 75% cis-1,4, 18% trans-1,4, and 7% 3,4 units for the PI50k and of 65% cis-1,4, 29% trans-1,4, and 6% 3,4 units for the PI3k, which was verified by NMR spectroscopy.

The weight-average molecular weights of the PI50k polymers were determined by low angle laser light scattering in heptane. The number-average molecular weight of the h-PI3k sample was obtained from ^{1}H NMR measurements using the 9 protons of the *tert*-butyl initiator group as internal reference. Size exclusion chromatography (SEC) on the d-PI3k and h-PI3k in THF revealed almost identical elution volumes. The molecular weight of the d-PI3k is then derived from the number-average molecular weight of the h-PI3k obtained by NMR multiplied by the ratio of the molecular weights of the monomeric units, 76/68. The polydispersity of all PIs were determined by size exclusion chromatography (SEC) in THF relative to polystyrene standards. After saturation all PEP materials were remeasured by SEC revealing no detectable change in polydispersity. For the h-PEP materials complete saturation was verified by the disappearence of the vinyl protons in the ^{1}H NMR spectra. Complete saturation was also assumed for the d-PEP polymers since they were prepared identically. The average molecular weights of the final PEP polymers were then recalculated by the simply adding D_2 or H_2 per repeat unit. The characteristics of all PEP polymers are summarized in Table 1.

The silica nanofillers were obtained from Nissan Chemical (trade name: ORGANOSILICASOL Tol-St), and will be referred to as "ST" particles in this work. According to supplier information, the particle diameter is $D_{ST} \approx 10-15$ nm; the silica surface is partially modified with short hydrocarbons not specified further. Approximately 20% of the OH surface groups have been replaced, which suffices to render the particle hydrophobic. The silica are supplied in a stable toluene solution at a filler fraction of $\Phi = \Phi_{ST} \approx 30$ vol %. For a more accurate specification of the particles, we conducted an elemental analysis, yielding the element abundances given in Table 2. Moreover, none of the supplier informations were used in the evaluation of the experiments. All necessary particle parameters were determined in adequate experiments, the results of which are given in the text.

Both PEP and the particle surface layer consist of hydrocarbons. Thus, a dominantly repulsive particle−polymer interaction is realized and the PEP-ST system constitutes a model nanocomposite with repulsive interactions. The only nonrepulsive forces are due to van der Waals attraction.

The samples are divided into two different species: PEP−silica nanocomposites and silica solutions in toluene. A complete list of

Table 2. Elemental Analysis of the Tol-St Particles

element	Si	O	H	C
mass fraction	0.46	0.45	0.01	0.08
number fraction	0.26	0.45	0.19	0.10

Table 3. Sample Nomenclature[a]

sample	Φ_{Si} [vol %]	ratio h-/d-tol	ratio h-/d-PEP
PEP3k-0	0		52/48
PEP3k-35	35		52/48
PEP3k-50	50		52/48
PEP3k-60	60		52/48
PEP50k-0	0		52/48
PEP50k-18	18		52/48
PEP50k-35	35		52/48
PEP50k-50	50		52/48
Si33	0.75	33/67	
Si38	0.75	38/62	
Si46	0.75	46/54	
Si56	0.75	56/44	
Si66	0.75	66/34	
Si100	0.75	100/0	
hd-tol27	27	57/43 = ρ_{part}	

[a] PEP50k denotes the $M_w \approx 50$ kg/mol polymer matrix and PEP3k the $M_w \approx 3$ kg/mol matrix. All values refer to the temperature used in the corresponding measurement, i.e., $T = 150$°C for the nanocomposites and room temperature for the solution samples. The h/d ratios of protonated vs. deuterated components are given in vol/vol.

sample compositions is given in Table 3. The nanocomposites were obtained by means of solution mixing in toluene. After stirring for 48 h, the samples were first evaporated in air for 12 h and then dried in a vacuum oven for 48 h at $T = 50$ °C. In order to minimize oxigen residues, the dry samples were loaded into copper sample containers (thickness = 1 mm) for the SANS measurements under argon conditions. The silica solution samples were also stirred for 48 h and then filled into glass containers (thickness = 1 mm). The vessels were sealed with Parafilm in order to prevent solvent evaporation.

Methods: Small Angle Neutron Scattering (SANS). The SANS experiments were performed on the KWS-2 SANS instrument of the Jülich Centre for Neutron Science (JCNS) at the FRM II research reactor in Garching, München, Germany. The polymer and nanocomposite samples were measured at a temperature of $T = 150$ °C. Three different setups with sample-to-detector distances of $L = 2$ and 8 m for $\lambda = 7$ Å and $L = 8$ m for $\lambda = 12$ Å were used. For all setups a 8 m collimation length was used. The wavelength spread was $\Delta\lambda/\lambda = 20\%$. With these setups the scattering vector Q covers a maximum range of 2×10^{-3} Å$^{-1} \leq Q \leq 0.2$ Å^{-1}. The silica dispersed in toluene samples were measured at room temperature using two different setups with sample-to-detector distances of $L = 2$ and 8 m for $\lambda = 7$ Å. The raw data were corrected for the detector sensitivity, background noise and scattering from the empty cell, and calibrated in absolute units (cm^{-1}) by using a PMMA secondary standard according to:

$$\left(\frac{d\Sigma}{d\Omega}(Q)\right)^{s} = \frac{(L^{s})^2 h^{pl} T^{pl} (d\Sigma/d\Omega)^{pl}}{(L^{pl})^2 h^{s} T^{s} T^{ec} \langle I^{pl} \rangle} ((I^{s}(Q) - I^{bc})(Q) - T^{s}(I^{ec}(Q) - I^{bc}))$$

Here pl, s, ec, and bc refer to the PMMA standard, sample, empty cell, and boron carbide, respectively. T denotes the transmission, $I(Q)$ the scattered intensity, h the sample thickness, L the sample-to-detector distance and $\langle I^{pl} \rangle$ the averaged measured intensity of the PMMA. After radial averaging the calculated incoherent contribution of the protonated chains/protonated toluene was subtracted in order to obtain the absolute normalized macroscopic differential cross sections $(d\Sigma/d\Omega)(Q)$, hereafter abbreviated as $I(Q)$.

The determination of the incoherent background was realized differently for the solution and the polymer samples. In the particle−toluene solutions, the scaled measured toluene background $(1 - \Phi_{Si})[\eta_h (d\Sigma/d\Omega)_{htol} + (1 - \eta_h)(d\Sigma/d\Omega)_{dtol}]$ was subtracted, where η_h is the fraction of protonated toluene in the sample (cf. Table 3). The scattering cross sections of protonated toluene $(d\Sigma/d\Omega)_{htol}$ and deuterated toluene $(d\Sigma/d\Omega)_{dtol}$ were determined separately by SANS measurements of the pure, unfilled solvents.

In the unfilled polymer melts PEP3k-0 and PEP50k-0 the determination of the incoherent background $(d\Sigma/d\Omega)_{inc,\,PEP}$ was performed in a different manner. A constant value $C_{inc,0}$ was subtracted from the data and optimized to yield a regime of linear slope at high Q (in the usual double logarithmic presentation). The obtained best fit value for $C_{inc,0}$ was then compared to the measured scattering cross section of protonated PEP scaled with the corresponding volume fraction, $0.52(d\Sigma/d\Omega)_{hPEP}$. The values were found to be in good agreement with slight deviations due to the incoherent contribution from dPEP, which was not separately measured.

For the nanocomposites, an analogous procedure was used. A value $C_{inc}(\Phi)$ was subtracted from the corresponding data curve and optimized to yield a regime of linear slope at high Q. The resulting values were found to fulfill the relation $C_{inc}(\Phi) \approx (1-\Phi)C_{inc,0}$ in good approximation and thus accepted. The slight deviations from the relation are in accordance with an additional, small incoherent background from the protonated particle surface. Note that from the resulting uncertainty of $C_{inc}(\Phi)$ a maximal error of ± 0.05 is introduced in the analysis of high-Q slopes, which will later in this work be employed to characterize the chain size and statistics.

Theoretical Background

In order to analyze the scattering diagrams a brief review of the necessary theory is given. The scattering cross section $d\Sigma/d\Omega =: I(Q)$ is defined by

$$I(Q) = \langle |A(Q)|^2 \rangle = \langle | \sum_j b_j \exp(i\vec{Q}\vec{r}_j) |^2 \rangle \quad (1)$$

$A(Q)$ denotes the scattering amplitude and b_j the atomic scattering length, and the momentum transfer Q is given by

$$Q = \frac{4\pi}{\lambda} \sin(\vartheta/2)$$

where ϑ denotes the scattering angle.

The scattering function of an ideal Gaussian chain is given by (e.g., in ref 11)

$$I_{pol}(Q) = V \Phi_{pol} \Delta\rho^2 S_{pol}(Q) = V \Phi_{pol} \Delta\rho^2 \frac{1}{N^2} \left\{ N \frac{1+b}{1-b} - 2b \frac{1-b^N}{(1-b)^2} \right\} \quad (2)$$

where $S_{pol}(Q)$ is the single chain structure factor, N is the number of Kuhn monomers and $b = \exp(-l_K^2 Q^2/6)$ with the Kuhn length l_K. V is the volume of a polymer chain, Φ_{pol} the polymer volume fraction, $\Delta\rho = \rho_1 - \rho_2$ the scattering contrast with ρ_i $(i = 1,2)$ the corresponding scattering length densities (=:SLD) of polymer and matrix or solvent.

For large N, $S_{pol}(Q)$ can be simplified to the Debye formula

$$S_{Debye}(Q) = \frac{2}{x^2}(x - 1 + \exp(-x)) \quad (3)$$

with $x = Q^2 R_g^2$, where the radius of gyration is given by $R_g^2 = \int r^2 \rho(\vec{r})\, d^3r / \int \rho(\vec{r})\, d^3r = C_\infty n l_0^2$ with distance from the center of

mass r, SLD ρ, backbone bond number $n = N_{mono}n_b$, where N_{mono} is the number of monomers per chain and n_b the number of backbone bonds per monomer ($n_b = 3.85$ for the PEP structure in this work), bond length l_0 (≈ 1.54 Å for C−C single bonds) and characteristic ratio C_∞.

In a polymer isotope blend, the protonated ("p") and deuterated ("d") species of the polymer also have energetic interactions that can be accounted for via the (nondimensional) Flory−Huggins parameter χ by a random phase approximation:[11]

$$\frac{\Delta\rho^2}{I(Q)} = \frac{1}{\Phi_p V_p N_p S_p(Q)} + \frac{1}{\Phi_d V_d N_d S_d(Q)} - 2\chi/V_0 \qquad (4)$$

Here Φ_i, V_i, and N_i are the corresponding volume fraction, monomer volume, and degree of polymerization of the two isotopes and V_0 is the average monomer volume.

The χ parameter of a blend of protonated and deuterated PEP was determined separately by an analysis of PEP blends at different h/d ratios and yielded $\chi = (5.4 \pm 0.8) \times 10^{-3}$. This value is close to zero, but will be used nevertheless in the evaluation of polymer conformations in this work. More importantly, however, eq 4 enables us to include the different degrees of polymerization N_p and N_d of protonated and deuterated species in the analysis, which are a consequence of the desire to achieve equal molecular weights $M_{w,h} \approx M_{w,d}$ for the two species.

In the case of solid identical, spherical, monodisperse particles, the cross section can be factorized

$$I(Q) = V\Phi\Delta\rho^2 S(Q)P(Q) = \frac{\Phi}{V} S(Q)\langle|A_{part}(Q)|^2\rangle \qquad (5)$$

where V is the volume of the scattering particle. Φ denotes the corresponding volume fraction and $\Delta\rho = \rho_1 - \rho_2$ the scattering contrast with ρ_i ($i = 1, 2$) the corresponding scattering length densities (SLD) of the different sample components. $P(Q)$ is the form factor of 1 particle, $A_{part}(Q)$ the scattering amplitude of one particle according to eq 1, and $S(Q)$ the structure factor, which contains the pair correlations of the particle centers. In a dilute system, $S(Q) = 1$.

The nanoparticles are assumed to be spherically symmetric. The form factor of a sphere is given by[12]

$$P_{sphere}(Q, R) = \left[\frac{3}{x^3}(\sin(x) - x\cos(x))\right]^2 \qquad (6)$$

where $x = QR$ with particle radius R.

Instead of a simple spherical structure with homogeneous density, several papers suggested a core−shell structure for the description of silica particles grafted with organic molecules.[13] This issue will also be addressed. For a spherical core−shell particle (see inset Figure 2b) with core radius R, shell thickness t and scattering length densities ρ_{co} and ρ_{sh} in a solvent with SLD ρ_{so}, it is found that

$$A_{co-she}(Q) = \Delta\rho_{co} V_{co} B_{co}(Q) + \Delta\rho_{sh} V_{sh} B_{sh}(Q) \qquad (7)$$

where V_i denotes the corresponding scattering volume, $\Delta\rho_i = \rho_i - \rho_{so}$, $B_{co}(Q) = 3/x^3(\sin(x) - x\cos(x))$ is the core amplitude, and $B_{sh}(Q) = 3/(y^3 - x^3)[(\sin(y) - y\cos(y)) - (\sin(x) - x\cos(x))]$ the shell amplitude with $x = QR$ and $y = Q(R + t)$.

The formulas so far are valid for monodisperse particles. A particle size distribution according to a normalized distribution function $f(r)$ is included in this work via a local monodisperse approximation:

$$I(Q) = \int_0^\infty f(r)P(Q, r)S(Q, r)\,\mathrm{d}r \qquad (8)$$

For $S(Q,r) = 1$, the formula is exact.

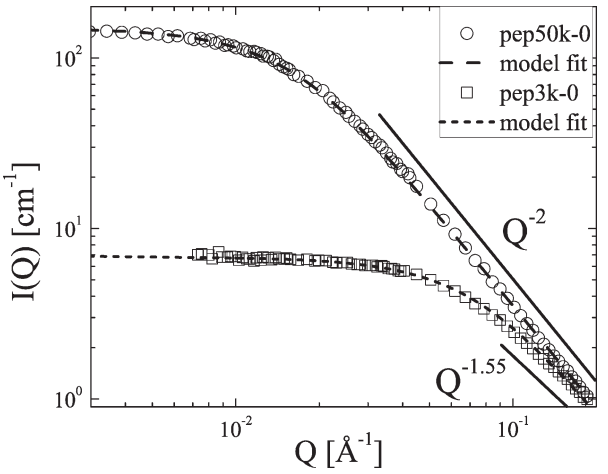

Figure 1. Single chain form factors of PEP3k-0 and PEP50k-0 with fits.

In the context of this work, a log-normal distribution will be used,

$$f(r) = \frac{1}{\sqrt{2\pi}\sigma r} \exp\left(\frac{\ln(r/R_{med})}{2\sigma^2}\right) \qquad (9)$$

The median R_{med} and width σ of the distribution are related to the expectation value $R_{avg} := \langle r\rangle$ and variance Var(f) via $R_{avg} = R_{med}\exp(\sigma^2/2)$ and $\mathrm{Var}(f) = R_{med}^2(\exp(2\sigma^2) - \exp(\sigma^2))$.

Results and Discussion

Characterization of the Pure Polymer Melts. In Figure 1, the scattering curves of the unfilled polymer melts PEP50k-0 and PEP3k-0 are shown on the absolute scale. The error bars are within the symbol size and therefore left out for the sake of clarity. The lines represent fits using the model functions, eq 2 for PEP3k and eq 3 for PEP50k, including a random phase approximation according to eq 4.

To reduce the degrees of freedom in the fitting procedure, the radius of gyration of the deuterated PEP $R_{g,d}$ was coupled to the protonated PEP $R_{g,p}$ via the known ratio of monomer numbers N_i ($i = p, d$)

$$R_{g,d} = R_{g,p}\sqrt{N_p/N_d}$$

In the case of PEP50k the radius of gyration for the protonated species $R_{g,p,50k} = 8.33 \pm 0.03$ nm was obtained, yielding a characteristic ratio $C_\infty = 6.45 \pm 0.05$ at $T = 150$ °C. Zirkel et al. found $C_\infty = 6.51$ at $T = 150$ °C[14] in good agreement with the results here. At high Q values perfect Q^{-2}-behavior is observed, characteristic for unperturbed Gaussian chain statistics and in accordance with the Debye formula.

In the case of the low M_w sample, finite size effects are visible because of the low monomer number $N_{mono} = 43$. We have to use the exact eq 2 in the random phase approximation 4, yielding $R_{g,p,3k} = 1.93 \pm 0.03$ nm, and accordingly $C_\infty = 5.7 \pm 0.2$. By means of RIS theory Zirkel et al. have calculated values of $C_N(T = 120\ °C) \approx 6.00$ and $C_N(T = 250\ °C) \approx 5.35$ for $1/N = 0.025$.[14] By linear extrapolation, $C_N(T = 150\ °C) \approx 5.86$ can be estimated, which is in good agreement with the value found here. In the high-Q regime a $Q^{-1.55}$-behavior is observed. This is not, however, a deviation from ideal Gaussian chain behavior, but only a consequence of the low monomer number. The slope −1.55 is reproduced by the unapproximated scattering eq 2.

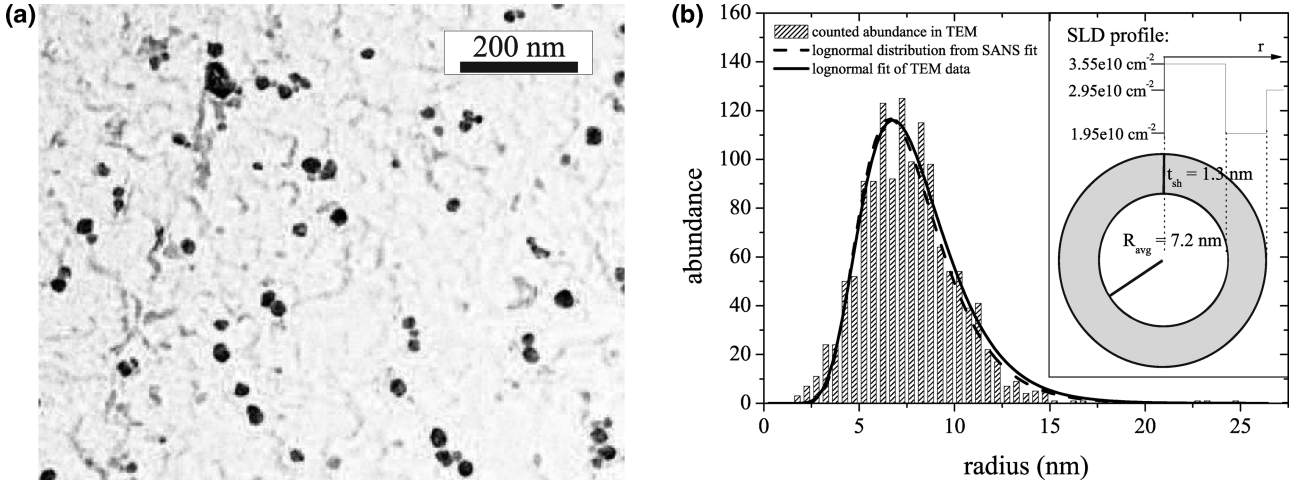

Figure 2. (a) TEM micrograph of silica primary particles. Smeared regions are artifacts from the object carrier. (b) Histogram of core radii from the TEM images with a log-normal fit (black line); the green line is the log-normal distribution of core radii from the SANS measurements; the inset is a sketch of the core−shell model structure with the corresponding profile of scattering length densities.

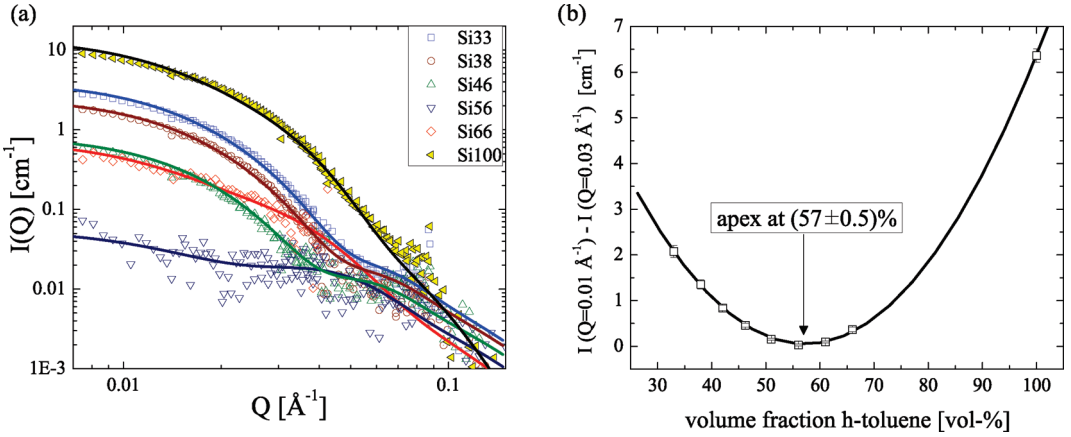

Figure 3. (a) 0.75 vol % ST in hd-toluene with core−shell fits (see text). (b) Contrast parabola of ST in hd-toluene.

In summary, the single chain form factors of the unfilled PEP melts can be very accurately modeled by ideal unperturbed Gaussian chains.

Characterization of the Particle Phase. For the characterization of the silica particles, transmission electron microscopy (TEM) and SANS were used. In the TEM experiments, the supplied solution was diluted to about 0.8% (w/w), dropped on a carbon coated copper grid and dried in high vacuum. The measurements were done with a Philips CM 200 TEM at an operating voltage of 200 kV. The sizes of 1835 particles were evaluated in order to characterize the silica primary particle diameters. Figure 2a shows an exemplary micrograph. In Figure 2b, a histogram with the prevailing particle radii is given. The best fit was achieved by a log-normal distribution with average particle radius $R_{avg} = (7.90 \pm 0.08)$ nm and $\sigma = 0.32$ (solid line in the figure). This is in good agreement with the supplier information $D_{Si} \approx 10-15$ nm.

A more detailled characterization of the particles, including information about the organic surface shell, is possible by SANS measurements. Additionally, the scattering length density of the particles has to be determined in order to be able to contrast match them in SANS experiments with nanocomposites.

Figure 3a shows the results of a SANS contrast variation study with 0.75 vol % silica in a mixture of protonated and deuterated toluene (-d_8). The lines in the figure represent fits, which will be explained in detail below. In order to determine the contrast matching condition, the intensity at a given Q-value is evaluated as a function of the mean scattering length density of the solvent. This should result in a parabola in accordance with eq 5. The parabola apex is then the average SLD of the particle. The result of this approach for the ST particles is plotted for a single Q value in Figure 3b), yielding an average SLD $\rho_{ST} = (2.95 \pm 0.05) \times 10^{10}$ cm^{-2}. This value is significantly smaller than $\rho_{SiO2} \approx (3.55 \pm 0.08) \times 10^{10}$ cm^{-2} calculated for amorphous SiO_2 with a mass density of 2.25 ± 0.05 g/cm^3.

Furthermore, a Guinier analysis was performed to extract the radius of gyration $R_{g,app}$ of the particles from each of the data sets in Figure 3a. A significant variation of the extracted apparent $R_{g,app}$ of the ST particles with solvent SLD is found here. Figure 4 shows that approximately $R_{g,app}^2 \propto 1/\Delta\rho$, where $\Delta\rho = \rho_{ST} - \rho_{solv}$. For a homogeneous particle the apparent value of R_g must be constant, and in particular independent of the solvent SLD. This indicates that the surface modified ST particles cannot be modeled as homogeneous hard spheres.

Complete contrast matching is not possible, if the particles are not homogeneous. In this particular case, the nanofillers consist of a silica core and an organic surface with differnt SLDs. The observed dependence $R_{g,app}^2 \propto 1/\Delta\rho$ is in accordance with calculations by Markovic et al.[15] for spherical core−shell particles.

As a consequence, the scattering curves in Figure 3a must be described with a core−shell model (eq 7). Furthermore,

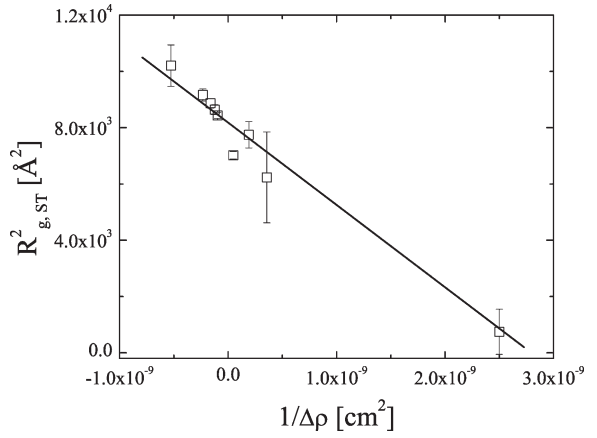

Figure 4. Apparent R_g^2 from Guinier fits vs $1/\Delta\rho$ according to ref 15.

the previously determined SLD ρ_{ST} must be perceived as an average particle SLD

$$\rho_{ST} = (V_{co}\rho_{co} + V_{sh}\rho_{sh})/V_{ST} \quad (10)$$

(with the indices signifying core, shell and the whole particle). The particle core is assumed to consist of typical amorphous silica with a density of 2.25 g/cm^3, yielding $\rho_{co} = 3.55 \times 10^{10}$ cm^{-2}. The shell is assumed to consist of the organic surface groups ($\rho_{CH_2} \approx 0$ cm^{-2}). Furthermore, it is not excluded that the silica particles are less compact at the periphery. Thus, a less compact silica fraction ($\rho_{SiO_2} \leq 3.55 \times 10^{10}$ cm^{-2}) will also be included in the shell. The average shell SLD value ρ_{sh} is expected to be well in between these limits. Moreover, it has to be pointed out that the scattering curves do not display a clear Guinier regime at low Q, but show slight forward scattering. Meyer et al. showed for very similar particles in a combined SANS/TEM study that this is due to an aggregation of silica primary particles with an average aggregation number $N_C \approx 2$.[16] This is accounted for by the structure factor $S_{SH}(N_C,Q)$ calculated by Schweins and Huber,[17] adapted to reflect aggregates of touching hard spheres. Note that in the analysis of[16] as well as in this work, N_C is included as an effective and experimentally evaluated aggregation number. In reality, the TEM analysis points to a narrow distibution of the aggregation number within different aggregates around an average value N_C, justifying the procedure.

By using eq 8 and a log-normal distribution of core diameters (mean core radius R_{avg} and polydispersity σ) as motivated by the TEM investigations, the experimental data in Figure 3a are described by one joint fit. The fits are in good agreement with the experimental data in all cases (see solid lines in Figure 3a), providing a core radius $R_{avg} = 7.2 \pm 0.1$ nm, and a shell thickness $t_{sh} = 1.3 \pm 0.1$ nm. All extracted parameters are given in table Table 4. Note that within the experimental accuracy the results consistently reproduce (via eq 10) the average SLD $\rho_{ST} = 2.92 \times 10^{10}$ cm^{-2} $\approx (2.95 \pm 0.05) \times 10^{10}$ cm^{-2} found before.

The log-normal distribution of particle core diameters is compared to the results of the TEM analysis in Figure 2b). The solid line is the result from the TEM histograph with $R_{avg,TEM} = 7.9$ nm and $\sigma_{SANS} = 0.32$, whereas the dashed line is a log-normal distribution with $R_{avg,SANS} = 7.2$ nm and $\sigma_{SANS} = 0.32$. The results from the two methods are in excellent agreement, with small deviations supposedly arising from the different contributions of the surface shell in the two methods.

Polymer Structure in Dependence of Filler Fraction Φ. *PEP3k-ST Composites*. The scattering results from the short chain PEP3k-ST nanocomposites for various particle fractions are shown in Figure 5a. The ratio of protonated to deuterated PEP was always chosen as 52/48 in volume to reproduce the mean silica SLD at 150 °C. Three features are visible.

1 A strong excess forward scattering at low Q.
2 The appearance of a peak at intermediate Q.
3 The collapse to one master curve of the different results at high Q, if the data are scaled with the polymer volume fractions $\Phi_{pol} := 1 - \Phi$ of the samples.

Table 4. Particle Properties from SANS

R_{avg}	7.2 ± 0.1 nm
σ	0.32 ± 0.02
t_{sh}	1.3 ± 0.1 nm
ρ_{co}	3.55×10^{10} cm^{-2} (fixed)
ρ_{sh}	$(1.95 \pm 0.1) \times 10^{10}$ cm^{-2}
N_C	2 (fixed)
Φ	0.75% (fixed)

These observations agree with those found by Sen et al. for the case of polystyrene filled with silica nanoparticles.[10]

First, we address the high-Q regime, because an analysis of the radii of gyration in the intermediate and low-Q regime is impossible due to the significant peak structure in this region. In the Kratky regime at high $Q \gg Q_{peak}$, for Gaussian chains the polymer scattering intensities of two different nanocomposite samples can be related to the statistical segment length l_K via

$$\sqrt[m]{\frac{I(\Phi_{p1},Q)/\Phi_{p1}}{I(\Phi_{p2},Q)/\Phi_{p2}}} = \frac{l_{K,\Phi_{p2}}}{l_{K,\Phi_{p1}}} = \frac{R_{g,\Phi_{p2}}}{R_{g,\Phi_{p1}}} \quad (11)$$

where $\Phi_{p1,p2}$ is the corresponding polymer volume fraction. For ideal chains with $N \rightarrow \infty$, where the Debye eq 3 is applicable, $m = 2$.[18] For very short chains, the equation is approximate and $m < 2$ is found from eq 2.

This relation can be even better visualized in a Kratky-like plot, i.e. $I/\Phi_{pol}Q^{1.55}$ vs Q (cf. Figure 5b), because then the high Q regime appears as a horizontal line for the unfilled sample PEP3k-0. In the figure, it is obvious that for $Q > 0.08$ Å^{-1}, all curves collapse to a common plateau. This indicates that neither R_g nor the chain statistics are altered by the presence of the nanoparticles. These findings agree very well with those of Sen,[10] who found no change of the single chain conformation in SANS experiments on a PS−silica system with PS chain lengths $N_{mono} > 860$.

Furthermore, also the simulations of nanocomposites presented in the introduction agree with the observations. Picu and Ozmusul[6,7] showed that for short chains neither the size nor the statistics of a polymer chain is affected.

We also want to hint at results found in a simulation of polymers confined between smooth walls by Li et al.[19] He shows that R_g^2 starts to decrease significantly, as soon as the wall separation distance is on the order of the polymer radius of gyration. In the case of the PEP3k chains, $R_g \approx 1.9$ nm, which is smaller than the typical void size in the present hard sphere system of spheres with diameter $D_{ST} = 17$ nm (for detailled void size calculations refer, e.g., to ref 20).

At intermediate values of Q a peak is visible, which becomes more prominent with increasing Φ. The peak position $Q_{peak} = 0.04$ Å^{-1} corresponds to a correlation length of $\xi_{3k} = 2\pi/Q_{peak} \approx (16.0 \pm 0.3)$ nm $\approx D_{ST}$. From the assumption of additivity of scattering contributions a first quantification of the peak can be achieved by introducing the peak height $H_{3k}(\Phi) = I(\Phi,Q_{peak}) - \Phi_{pol}I(\Phi = 0,Q_{peak})$. Values of H are given in table Table 5. It is found that in good approximation $H_{3k}(\Phi) \propto \Phi$ (cf. Figure 6). A more detailled discussion of the intermediate Q peak will be given later in this work.

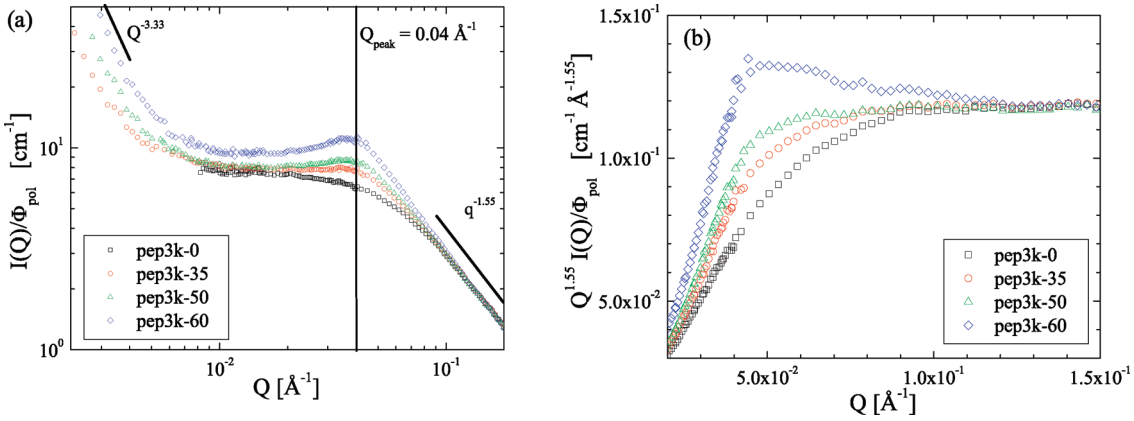

Figure 5. PEP3k SANS curves, normalized to Φ_{pol}, represented at different filler degrees: (a) double logarithmic plot; (b) Kratky-like scaling.

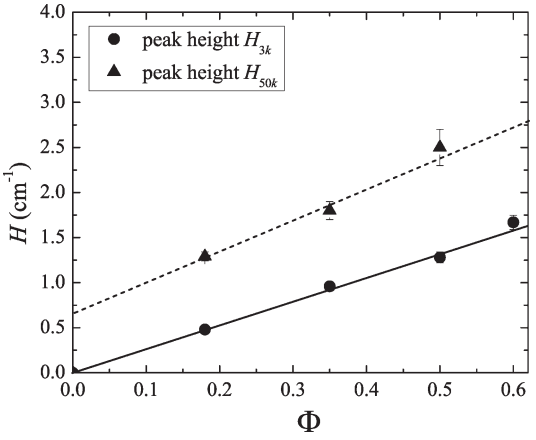

Figure 6. Peak heights $H_{3k}(\Phi)$ (○) and $H_{50k}(\Phi)$ (▲) vs silica fraction Φ. The lines are linear fits.

Table 5. Peak Heights $H_{3k}(\Phi)$ and $H_{50k}(\Phi)$

Φ (%)	$H_{3k}(\Phi)$ (cm^{-1})	$H_{50k}(\Phi)$ (cm^{-1})
18		1.29
35	0.96	1.80
50	1.28	2.50
60	1.67	

In all the samples containing filler particles, strong forward scattering at low Q is observed. The slope of the forward scattering contributions is $d \approx -3.33$ in all cases, the amplitudes vary systematically with filler fraction. The existence of strong forward scattering can be rationalized by scattering from holes and silica aggregates. A more quantitative analysis of this low-Q feature is not envisaged in the frame of this work, however.

PEP50k-ST Composites. In Figure 7a, the SANS data of the higher molecular weight PEP50k-ST nanocomposite series is plotted. At low Q, again strong forward scattering possibly due to particle aggregates and holes is visible, yet not further discussed in more detail here.

Moreover, at high $Q > 0.1$ Å^{-1} all curves show in good approximation the same Q^{-2} dependence that was observed in the unfilled polymer melt already. This means that the chain statistics are largely unperturbed on small length scales, which is again best illustrated in Kratky scaling (Figure 7b). The Kratky plateaus are parallel, but do not coincide, if normalized with Φ_{pol}. The latter indicates a change of the average radius of gyration $R_{g,50k}(\Phi)$. Since there is no significant contribution of the scattering peak in this Q regime, eq 11 can be used to directly extract the corresponding ratios $R_{g,ratio} := R_g(\Phi)/R_g(\Phi = 0)$ from the ratio of the Kratky plateau values. An increase of the plateau level is equivalent a decrease in R_g. A quantification of the effect is given in table Table 6.

Having determined $R_g(\Phi)$, we can now compute the theoretical curve $I_{theo}(R_g(\Phi))$ of a Gaussian chain with radius of gyration $R_g(\Phi)$. In the calculation, all parameters except R_g were taken from the best model fit of the unfilled sample PEP50k-0, which is shown in Figure 1. $I_{theo}(R_g(\Phi))$ was then calculated by means of a random phase approximation (eq 4) with polymer single chain structure factor $S_{pol}(Q)$ according to eq 3. This is the same model calculation that was also used for the description of the chain conformation in the unfilled PEP melt. For $\Phi = 50\%$, the corresponding model curve is shown in Figure 8 in absolute units. The analogous descriptions of the $\Phi = 18\%$ and $\Phi = 35\%$ data are vertically shifted in the figure for the sake of clarity. (The data were shifted by the same factor in order to preserve the comparison between data and model calculation.) Both high and low Q data of the samples are in good agreement with $I_{theo}(Q)$. We conclude that the chain statistics is not affected, whereas a decrease of R_g is observed. In particular, the polymer conformation is still Gaussian.

The same behavior was also found in a simulation of polymers between smooth walls by Li et al,[19] where it is shown that R_g decreases, when the wall separation distance is on the order of R_g or less.

Furthermore, Sharaf[5] conducted MC simulations of $d = 20$ nm particles in a melt of polyethylene chains. The degree of polymerization is similar to N_{mono} of the PEP50k chains used here. He did not account for any adsorption, making his system effectively nonattractive as in our case. He, too, found a slight, yet not very pronounced decrease of R_g. Vacatello[3] found in his MC simulations of polymer particle nanocomposites that in all cases a decrease of R_g was present. This decrease was always on the order of few percent, in accordance with the SANS results presented here. Furthermore, we want to point out the good agreement with the simulation results by Picu and Ozmusul.[6,7] They reported unaffected polymer chain sizes, when $R_g < r_{part}$, whereas the chain size decreased, when $R_g \gtrsim r_{part}$. This is exactly, what is observed in the present experimental study of the repulsive PEP-ST nanocomposite system.

As already witnessed in the low molecular weight samples, a scattering peak evolves with increasing Φ. The apparent peak position $Q_{peak} \approx 0.042$ Å^{-1} is almost identical with the PEP3k composites. It corresponds to a correlation length $\xi_{50k} = 15.0 \pm 0.3$ nm. Once again, a first quantification of the peak height can be achieved by defining

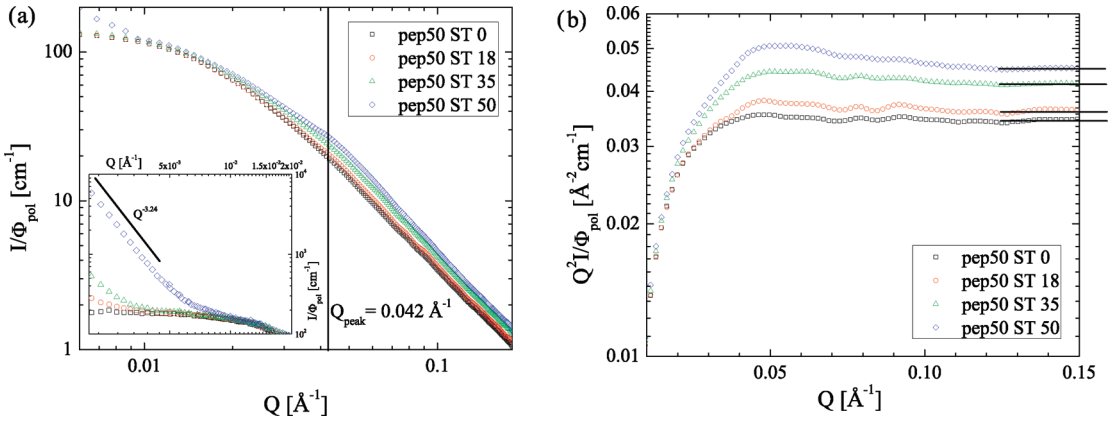

Figure 7. (a) PEP50k, various filler fractions. The inset shows the low-Q regime. (b) Kratky plot of the data for better visibility of the high-Q regime.

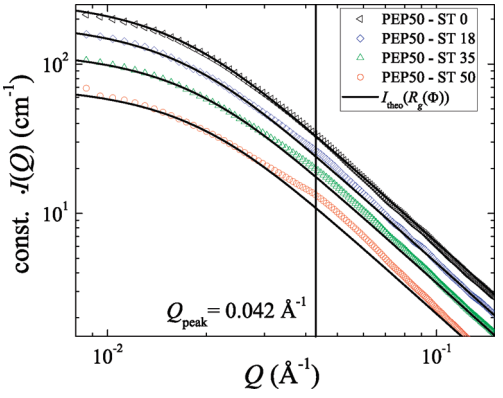

Figure 8. SANS data $I(Q)$ of PEP50k composites for different Φ. The solid lines are model calculations for $(1 - \Phi)I_{theo}(R_g(\Phi))$ (see text).

Table 6. $R_{g,ratio}(\Phi) := R_{g,avg}(\Phi)/R_{g,0}$ from the Kratky Plateau Analysis for PEP50k

Φ (%)	$R_{g,ratio}(\Phi)$
0	1
18	0.981 ± 0.005
35	0.922 ± 0.005
50	0.887 ± 0.005

$H_{50k}(\Phi) = I(\Phi,Q_{peak}) - \Phi_{pol}I_{theo}(R_g(\Phi),Q_{peak})$. In this case, however, the results will be less reliable, because the polymer scattering intensity of PEP50k is an order of magnitude higher than that of PEP3k, and consequently much more dominant compared to the structure peak in the high molecular weight matrix. Obviously the peak heights are different in the PEP3k and the PEP50k composites (by approximately a factor of 2), whereas the peak positions are nearly the same. The former quantitatively excludes that the peaks in the PEP3k and PEP50k composites are caused only by an identical particle contribution or only by an identical polymer correlation peak. If we were dealing with only a particle contribution, we would expect $H_{50k}(\Phi) = H_{3k}(\Phi)$.

hd-tol27. In order to quantify the scattering contribution due to the particles' core−shell structure, a study of a high volume fraction silica in a mixture of deuterated and protonated toluene at contrast matching conditions of the silica particles $\rho_{h/d-tol} = 2.95 \times 10^{10}$ cm$^{-2} = \rho_{h/d-PEP,composite}$ is very useful. Since the toluene molecules are very small compared to the silica particles, no voids and consequently no void scattering is expected.

In Figure 9, the resulting SANS data are plotted in absolute units. The prominent feature of the curve is a

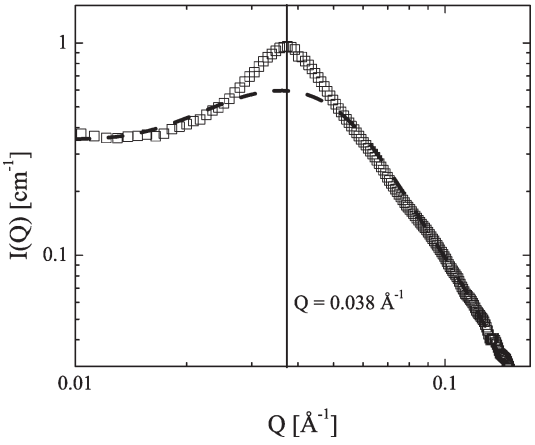

Figure 9. SANS data of sample hd-tol27. Dashed line: best fit with the Percus−Yevick model.

pronounced peak at $Q = 0.038$ Å$^{-1} \approx Q_{peak} = 0.04$ Å^{-1}. The peak cannot be modeled by a simple polydisperse Percus−Yevick hard sphere model (dashed line in Figure 9) as often applied in colloid solutions (e.g.,[21,22]). We have observed nearly constant peak positions at $Q_{peak} = 0.04$ Å^{-1} in all sample systems for all Φ. In a well-dispersed hard sphere system they should vary systematically with Φ.

Therefore, we rather propose to perceive the peak as due to an intracluster structure factor S_{intra}. S_{intra} is characteristic for a particle aggregate structure or the local colloidal cage structure of the silica respectively, where the curve shape changes only little in dependence of Φ. The associated correlation length is $\xi_{tol} \approx (16.5 \pm 0.3)$ nm, which is slightly bigger than the values found in the polymer nanocomposites. This slight dependence on silica "solvent" can be explained with respect to varied depletion interactions. The depletion interactions acting on the particles are stronger in the polymer samples than in toluene, leading to a slightly denser packed silica structure. The variation in peak positions is so small, however, that it will be neglected in first approximation for the further analysis.

Discussion: The Peak Structure. *PEP3k-ST Composites*. In the PEP−silica nanocomposites with both the short and long chain matrices, a peak at $Q_{peak} \approx 0.04$ Å^{-1} was observed. From the facts that $\xi \approx D_{ST}$, and that an analogous peak is observed in the scattering of sample hd-tol27 (cf. Figure 9), it can be concluded that the peak is in all cases due to the particle structure in the sample. The obvious connection to the particle structure does not, however, mean that the observed scattering signal is directly due to a particle contrast. Alternatively the particle structure

could lead to an imprint of correlations on the polymer phase. To clarify this issue, a closer inspection of the peak signal is necessary. It could in principle be due to three different sources:

1 In case of homogeneous filler particles and perfect contrast matching conditions, no scattering contribution from the particles themselves would be visible. Then the contribution could be interpreted as a polymer correlation peak. A prerequisite for its appearance, however, would be the existence of a scattering contrast within the polymer phase of the composite. This could, e.g., be due to a preferential localization close to the surface of either protonated or deuterated species, or to a polymer layer with slightly affected density close to the filler surface. In particular, the latter would be expected due to chain adsorption in systems with attractive polymer−particle interactions (see, e.g., refs 23−26 for experimental, simulative, and theoretical approaches), and was used in the experimental study by Sen et al. in a similar system to explain the existence of a scattering peak similar to the one present here.[10] In the case of the PEP3k-ST composites, however, no attractive interactions are expected. Moreover, the observation of unperturbed chain statistics and hardly affected dimensions makes an adsorbed phase of significantly altered density unlikely.
2 If the polymer chains were too bulky to populate the voids between particles, a void−void-correlation contribution from trapped argon within the particle aggregates would be present. With R_g = 2 nm chains and particle diameters of D_{ST} = 17 nm, this seems unlikely in the short chain system, though.
3 The third possible source of scattering is a direct contribution from the filler particles. If the particles were homogeneous, this explanation would require poorly matched samples. In the section above, however, we have proven that the core−shell nature of the particles contributes a significant scattering intensity to the overall signal. This contribution is almost nondistinguishable at low Φ, but may be very pronounced at high filler degrees, as is shown in Figure 9.

In order to address these issues, the contribution of the unmatched shell to the scattering diagram has to be evaluated. From the analysis of sample hd-tol27 (Figure 9) we are provided with information about the direct particle core−shell contribution at Φ = 0.27 in toluene at the same contrast conditions as in the polymer nanocomposites. We have shown that the scattering peak position is almost equal in all samples, $Q_{peak} \approx 0.04$ Å^{-1}, with only little dependence on the surrounding medium (toluene, PEP3k, PEP50k) and on filler fraction Φ. This is an indication that the intra cluster structure of the nanoparticles is very similar in all samples. Consequently the total scattering signal from the silica core−shell is expected to scale only with the absolute amount of particle content in the sample but is otherwise in good approximation equal in all investigated samples.

These considerations allow to approximate the direct silica contribution in the nanocomposite samples by the measured signal from Figure 9, weighted with the ratio of volume fractions Φ/0.27. Then, the scattering contribution from the silica can be directly removed from the nanocomposite data using the ansatz

$$I_{pol,3k}(\Phi) = I(\Phi) - \Phi/0.27 I_{hd-tol27} \qquad (12)$$

In the equation $I(\Phi)$ is the measured nanocomposite intensity, $I_{hd-tol27}$ that of 27 vol % ST particles in hd-toluene and

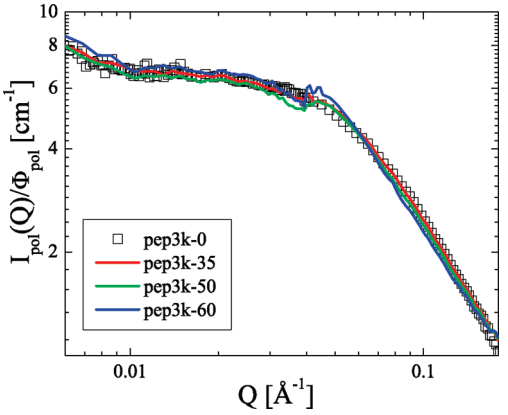

Figure 10. $I_{pol,3k}(\Phi)$ compared to data of PEP3k-0 sample. Good agreement yields quantitative proof that there is no visible polymer scattering contribution to the peak.

$I_{pol}(\Phi)$ the corrected scattering contribution of the polymer phase in the nanocomposite.

The curves for $I_{pol,3k}(\Phi)$ calculated in this way for the PEP3k samples are shown as solid lines in Figure 10. They are in very good agreement with the measured SANS data of the unfilled PEP3k sample, confirming that the chain conformations are not affected in this system. This confirms our previous deductions from the Kratky regime. Moreover the validity of the assumption that the internal particle aggregate structure factor is approximately independent of Φ and approximately the same in toluene and PEP3k seems justified. Finally, no significant polymer correlation peak or void correlation scattering is observed in the low molecular weight samples. The peak scattering contribution originates only from the core−shell scattering of particles in this system.

PEP50k-ST Composites. In the long chain nanocomposites, the first step toward a quantitative analysis is again the removal of the direct particle scattering. For that purpose the procedure defined by eq 12 was applied to the PEP50k nanocomposites. The result is shown in Figure 11. The curves are shifted by a constant factor for better visibility, the solid lines are the contributions from polymer single chain scattering $I_{theo}(R_g(\Phi))$ with the $R_g(\Phi)$ from table Table 6. Obviously the scattering peak is still present after removal of the direct particle scattering.

The remaining peak intensity may be either attributed to correlations in the polymer melt or to void correlation scattering. A quantitative decision for or against each of the two possibilities, however, requires additional experimental evidence and none of them can be unequivocally excluded from the data of the present study.

If the excess scattering signal is due to a polymer correlation peak, we can nevertheless deduce one important restriction from the SANS study, which will be briefly summarized here.

The idea of a region with perturbed polymer segment density near nanoparticles is supported by plenty computer simulations (see, e.g., refs 1 and 27). In particular, the mere existence of such a region is witnessed both in attractive as well as in nonattractive systems. Only the spatial range and significance of the density fluctuations depends on the attraction strength.

Moreover, Schweizer et al.[26,28] investigated the impact of nanoparticle presence on the polymer conformation by means of analytical PRISM calculations. Their results also show a change of the polymer segment−segment correlation near the particle surface, which would be seen in the scattering signal.

The physical origin of changed correlations is classified into two general effects by Schweizer:

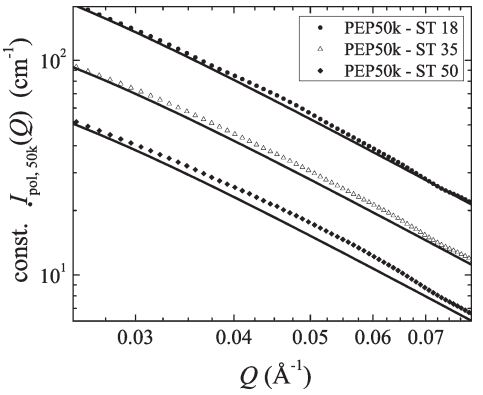

Figure 11. $I_{pol,50k}(\Phi)$ for different Φ in the intermediate Q regime. The solid lines are model calculations $I_{theo}(R_g(\Phi))$(see text); the scattering peak does not disappear completely.

(i) For one thing, there exists a purely entropical contribution, which is present even in nonattractive systems.[28] In this case, the disturbed segment−segment correlation is due to topological reasons. Nanoparticles cannot be pervaded by chains. Thus, the entropically favored chain organization close to the surface is not necessarily the same as in the bulk. The dominating correlation length for the consequent polymer density fluctuations is given by the particle dimensions, which is also observed in our experimental PEP-ST system. The impact of the effect is dependent on chain length. In particular, it is possible that there is a visible entropical contribution in the PEP50k system, whereas for the shorter PEP3k chains the contribution may be too small to be observed experimentally.

(ii) In nanocomposites with not too weak (phase separation!) and not too strong (particle−polymer network!) polymer−particle interactions the calculations by Schweizer show the existence of an adsorbed polymer layer with changed density near the particle surface.[26] This bound layer also leads to a polymer correlation peak, whose features are closely related to the particle parameters. Thus, the bound layer peak is qualitatively quite similar to the entropical peak from point i.

The peak position is predicted by the calculations at $Q_{peak,cal} = 2\pi/D_{part}$ in agreement with the results found here.

But according to ref 26, the strength of the bound layer peak is not dependent on chain length. Consequently, the arguments in point ii are not applicable to the PEP-ST system because of the absence of a polymer density fluctuation peak in the PEP3k-ST system.

It is still feasible that the remaining peak scattering signal in the PEP50k-ST composites may result from polymer density fluctuations. But the density change is then due to entropical reasons, which leads to perturbations of the polymer segment density near the nanoparticle surfaces.

Conclusion

In this work, it could be shown that a structural study of polymer nanocomposites by scattering methods necesseraly involves a thorough characterization of the incorporated filler particles. Otherwise, there is the risk of severe errors in quantitative as well as even qualitative interpretation of the results. This is in particular to be emphasized, because current model systems rely on particles with grafted surfaces in order to adjust the interactions in the systems.

The exact knowledge of the particle form factor and intra cluster structure factor were obtained in ancillary SANS measurements. The results were then used to quantitatively extract the origins of different contributions to the scattering pattern in a PEP−nanoparticle system with largely nonattractive filler−polymer interactions. When the chain size $R_{g,3k} = 2$ nm was much smaller than the particle radius $R_{ST} = 8.5$ nm, neither the chain statistics nor the average chain size was affected. This is in agreement with simulations by Li[19] and Picu.[6] Moreover, no evidence for a polymer correlation peak was observed. Instead, the appearance of a scattering peak at intermediate Q values could be unequivocally related to a scattering contribution from the core−shell structure of the particles.

When the unperturbed chain size $R_{g,50k} = 8.3$ nm was on the order of the particle radius $R_{ST} = 8.5$ nm, the chain statistics was still not affected, but the chains adapted a reduced radius of gyration with a minimal value of $0.887 \cdot R_{g,0}$. A decrease of R_g with increasing nanoparticle fraction was also found in numerous simulation studies (e.g., refs 3, 5, and 29).

Moreover, again a scattering peak with the same peak position as in the short chain samples was found. Subtraction of the direct particle contribution revealed the multiple origin nature of the peak. In addition to the particle core−shell contribution, void correlation scattering and a polymer correlation peak were identified as possible origins of the extra scattering intensity. The polymer correlation peak was related to PRISM calculations by Schweizer et al., with the restriction that in the experiments a polymer correlation peak was only present in the PEP50k-ST system, but not in the PEP3k-ST system. This contradicts the existence of a bound polymer layer and hints to a changed segment−segment-density due to entropical reasons.

In order to quantitatively decide the impact of void scattering vs polymer correlation peak, complementary methods will be needed.

Acknowledgment. K.N. gratefully acknowledges the financial support of the Evonik Stiftung.

References and Notes

(1) Termonia, Y. *Polymer* **2009**, *50*, 1062–1066.
(2) Sung, B. J.; Chang, R.; Yethiraj, A. *J. Chem. Phys.* **2009**, *130*, 124908.
(3) Vacatello, M. *Macromol. Theory Simul.* **2002**, *11*, 757–765.
(4) Vacatello, M. *Macromolecules* **2002**, *35*, 8191–8193.
(5) Sharaf, M. A.; Kloczkowski, A.; Sen, T. Z.; Jacob, K. I.; Mark, J. E. *Eur. Polym. J.* **2006**, *42*, 796–806.
(6) Picu, R. C.; Ozmusul, M. S. *J. Chem. Phys.* **2003**, *118*, 11239–11248.
(7) Ozmusul, M. S.; Picu, C. R.; Sternstein, S. S.; Kumar, S. K. *Macromolecules* **2005**, *38*, 4495.
(8) Nakatani, A. I.; Chen, W.; Schmidt, R. G.; Gordon, G. V.; Han, C. C. *Polymer* **2001**, *42*, 3713.
(9) Tuteja, A.; Duxbury, P. M.; Mackay, M. E. *Phys. Rev. Lett.* **2008**, *100*, 077801.
(10) Sen, S.; Xie, Y.; Kumar, S. K.; Yang, H.; Bansal, A.; Ho, D. L.; Hall, L.; Hooper, J. B.; Schweizer, K. S. *Phys. Rev. Lett.* **2007**, *98*, 128302.
(11) Higgins, J. S.; Benoit, H. C. *Polymers and Neutron Scattering*, Oxford University Press: Oxford, 3rd ed.; 2002.
(12) Lord Rayleigh *Proc. R. Soc. London, Ser. A* **1914**, *XC*, 219.
(13) Suzuki, T.; Endo, H.; Shibayama, M. *Langmuir* **2008**, *24*, 4537–4543.
(14) Zirkel, A.; Richter, D.; Pyckhout-Hintzen, W.; Fetters, L. J. *Macromolecules* **1992**, *25*, 954–960.
(15) Markovic, I.; Ottewill, R. H.; Cebula, D. J.; Field, I.; Marsh, J. F. *Colloid Polym. Sci.* **1984**, *262*, 648–656.
(16) Meyer, M. To be submitted for publication **2010**.
(17) Schweins, R.; Huber, K. *Macromol. Symp.* **2004**, *211*, 25–42.
(18) Jones, R. L.; Kumar, S. K.; Ho, D. L.; Briber, R. M.; Russell, T. P. *Macromol* **2001**, *34*, 559.
(19) Li, Y.; Dongshan, W.; Han, C. C.; Liao, Q. *J. Chem. Phys.* **2007**, *126*, 204907.
(20) Torquato, S.; Lee, S. B. *Physica A* **1990**, *167*, 361–383.

(21) Scheffold, F.; Mason, T. G. *J. Phys.: Condens. Matter* **2009**, *21*, 332102.
(22) Snook, I.; van Megen, W.; Pusey, P. *Phys Rev A* **1991**, *43*, 6900–6907.
(23) Anderson, B. J.; Zukoski, C. F. *Macromolecules* **2008**, *41*, 9326–9334.
(24) Zhang, Q.; Archer, L. A. *Langmuir* **2002**, *18*, 10435–10442.
(25) Smith, K. A.; Vladkov, M.; Barrat, J.-L. *Macromolecules* **2005**, *38*, 571–580.
(26) Hooper, J. B.; Schweizer, K. S. *Macromolecules* **2007**, *40*, 6998–7008.
(27) Starr, F. W.; Schroder, T. B.; Glotzer, S. C. *Phys. Rev. E* **2001**, *64*, 021802.
(28) Fuchs, M.; Schweizer, K. S. *J. Phys.: Condens. Matter* **2002**, *14*, R239–R269.
(29) Slater, G. W.; Nixon, G. I. *J. Chem. Phys.* **1998**, *108*, 3310–3312.